Biomaterials Science

ROYAL SOCIETY OF CHEMISTRY

PAPER

View Article Online
View Journal | View Issue

Cite this: *Biomater. Sci.*, 2024, **12**, 2136

Transplantation of a bioengineered tissue patch promotes uterine repair in the sheep†

Edina Sehic,[a,b] Lucía de Miguel Gómez,[a,b] Hardis Rabe,[c,d] Emy Thorén,[a,b] Ingigerdur Gudmundsdottir,[a,b] Mihai Oltean,[a,e] Randa Akouri,[a,b] Mats Brännström[a,b,f] and Mats Hellström *[a,b,c]

Innovative bioengineering strategies utilizing extracellular matrix (ECM) based scaffolds derived from decellularized tissue offer new prospects for restoring damaged uterine tissue. Despite successful fertility restoration in small animal models, the translation to larger and more clinically relevant models have not yet been assessed. Thus, our study investigated the feasibility to use a 6 cm^2 graft constructed from decellularized sheep uterine tissue, mimicking a future application to repair a uterine defect in women. Some grafts were also recellularized with fetal sheep bone marrow-derived mesenchymal stem cells (SF-MSCs). The animals were followed for six weeks post-surgery during which blood samples were collected to assess the systemic immune cell activation by fluorescence-activated cell sorting (FACS) analysis. Tissue regeneration was assessed by histology, immunohistochemistry, and gene expression analyses. There was a large intra-group variance which prompted us to implement a novel scoring system to comprehensively evaluate the regenerative outcomes. Based on the regenerative score each graft received, we focused our analysis to map potential differences that may have played a role in the success or failure of tissue repair following the transplantation therapy. Notably, three out of 15 grafts exhibited major regeneration that resembled native uterine tissue, and an additional three grafts showed substantial regenerative outcomes. For the better regenerated grafts, it was observed that the systemic T-cell subgroups were significantly different compared with the failing grafts. Hence, our data suggest that the T-cell response play an important role for determining the uterus tissue regeneration outcomes. The remarkable regeneration seen in the best-performing grafts after just six weeks following transplantation provides compelling evidence that decellularized tissue for uterine bioengineering holds great promise for clinically relevant applications.

Received 23rd November 2023,
Accepted 10th March 2024

DOI: 10.1039/d3bm01912h

rsc.li/biomaterials-science

1. Introduction

Infertility is an ongoing challenge and the World Health Organization estimates that more than 186 million people of reproductive age are affected.[1] Assisted reproductive technologies can often provide treatment solutions but some conditions remain challenging to overcome. Pioneering work include new therapies such as ovarian cortex transplantation that had been developed during the last decades as a methodology to preserve fertility following cancer treatment in young women.[2] Uterus transplantation has been established for women with a congenital or acquired uterine malformation.[3] Lately, various bioengineering strategies to treat infertility disorders concerning the ovary,[4,5] full thickness uterine tissue, endometrium, fallopian tube, and cervix showed encouraging preclinical results.[6] Bioengineered reproductive tissues may be derived from extracellular matrix (ECM) scaffolds obtained from respective decellularized tissue.[7,8] Pioneering uterus bioengineering work in a rat model indicated how such scaffolds entail a therapeutic alternative to regenerate damaged uterine tissue in a situation of significant defects following multiple cesarean sections or extensive myomectomy that causes infertility.[9–11] Extracellular matrix-derived scaffolds provide bioactive cues, structural support, and a low immuno-

[a]*Laboratory for Transplantation and Regenerative Medicine, Sahlgrenska Academy, University of Gothenburg, Kvinnokliniken, Blå stråket 6, SE-405 30, Sweden. E-mail: mats.hellstrom@gu.se; Tel: +46 766 184 572*
[b]*Department of Obstetrics and Gynecology, Clinical Sciences, Sahlgrenska Academy, University of Gothenburg, SE-405 30, Sweden*
[c]*Unit of Biological Function, Division Materials and Production, RISE – Research Institutes of Sweden, Box 857, SE-50115 Borås, Sweden*
[d]*Institute of Biomedicine, Department of Infectious diseases, Sahlgrenska Academy, University of Gothenburg, SE-405 30, Sweden*
[e]*Department of Surgery, Clinical Sciences, Sahlgrenska Academy, University of Gothenburg, SE-413 45, Sweden*
[f]*Stockholm IVF-EUGIN, Hammarby allé 93, 120 63 Stockholm, Sweden*
† Electronic supplementary information (ESI) available. See DOI: https://doi.org/10.1039/d3bm01912h

genicity, making them suitable for transplantation.[12–14] A whole ECM-derived uterus scaffold which is recellularized with the patient's own cells may also overcome some of the intrinsic disadvantages related to an allogenic uterus transplantation procedure, including the low donor organ availability, the risk of organ rejection and the negative side effects from immunosuppressive therapy.[15] Also, ECM exhibits tissue-specificity, featuring a proteome with distinct proteins and molecules that facilitate optimal behavior of the cells from the source tissue.[16] For these reasons, whole uterus ECM based scaffolds were created through decellularization for many species, including the mouse,[17] rat,[18–21] rabbit,[22] pig,[23] sheep,[24–26] and human.[27] Multiple independent labs showed fertility restoration in the rat model using small-sized uterine grafts, but these principles have not yet been evaluated in large animal models with a uterus of similar size as the human and thereby consisting of clinically relevant sized grafts.

We developed an ECM derived sheep uterus scaffold of reasonable size and transplanted it to replace an equally sized full-thickness uterine segment in the recipient sheep. Some developed grafts were also recellularized with fetal sheep bone marrow-derived mesenchymal stem cells (SF-MSCs) for their known immunomodulatory properties and to stimulate tissue regeneration after decellularized tissue transplantation in the rat model.[18] Blood samples were collected at regular intervals and small biopsies were assessed two weeks after surgery. The experiment was terminated six weeks following surgery to evaluate the graft properties, tissue regeneration and the host immune system response.

2. Materials and methods

2.1 Uterus isolation and decellularization

Sheep uteri were isolated from 8–12 months old female sheep (Swedish fin-ull and Dutch texel mixed breed) at a local abattoir. Animal ethics approval for this procedure was not needed since organs were collected from animals processed for food production. The uteri were taken to a nearby laboratory setting, and both uterine arteries were cannulated (20G, BD Neoflon, Becton. Dickinson GmbH, Heidelberg, Germany) and each uterus was perfused with ice-cold phosphate-buffered saline (PBS; Thermo Fisher Scientific, Stockholm, Sweden) supplemented with lidocaine (0.04 g l^{-1}; AstraZeneca, Gothenburg, Sweden) and heparin (5000 IU l^{-1}; Leo Pharma, Ballerup, Denmark), and then frozen in the same solution (−20 °C). The decellularization process started once the thawed organs had been connected to a perfusion pump that enabled vascular perfusion through the uterine arteries with decellularization reagents according to our previously published protocol.[25] In brief, each organ was perfused overnight at room temperature (RT) with 20 mM EDTA (Thermo Fisher Scientific) followed by a sodium deoxycholate solution (SDC 2%; Sigma-Aldrich, Stockholm, Sweden) for 8 h. Each organ was then perfused with deionized water (DW) for 26 h and PBS for 12 h, respectively, and by a 37 °C perfusion with DNase I for 1 h (8000 UI per organ; Sigma-Aldrich), and then, another washing step with DW for 26 h at RT. One more cycle with SDC, DW, DNase I, and the washing step was repeated as above. Each organ was then sterilized by the perfusion of peracetic acid for 1 h (0.1% diluted in NaCl), and then washed with sterile PBS until pH 7.0 was reached. The decellularized uteri were then frozen at −20 °C in sterile PBS until being prepared for engraftment. Segments, 2 × 3 cm in size, were excised under sterile conditions from thawed decellularized uterus tissue (Fig. 1A). To facilitate the subsequent recellularization step, each scaffold segment was enzymatically treated with activated matrix metalloproteinase 2 (MMP2; 2.5 μg L^{-1}, Sigma-Aldrich) and MMP9 (2.5 μg L^{-1}, Sigma-Aldrich) following a previously established scaffold preconditioning protocol.[26]

2.2 Sheep fetal bone marrow stem cell culture and scaffold recellularization

Sheep fetal bone marrow derived stem cells (SF-SCs) previously isolated and characterized[25] from passages 8–9 were expanded and cultured *in vitro* under standard conditions using DMEM Glutamax™ medium supplemented with Anti-Anti™ and 10% fetal bovine serum (FBS; Thermo Fisher Scientific). The cell concentration was adjusted to 20 × 10^6 cells in 3 mL culture

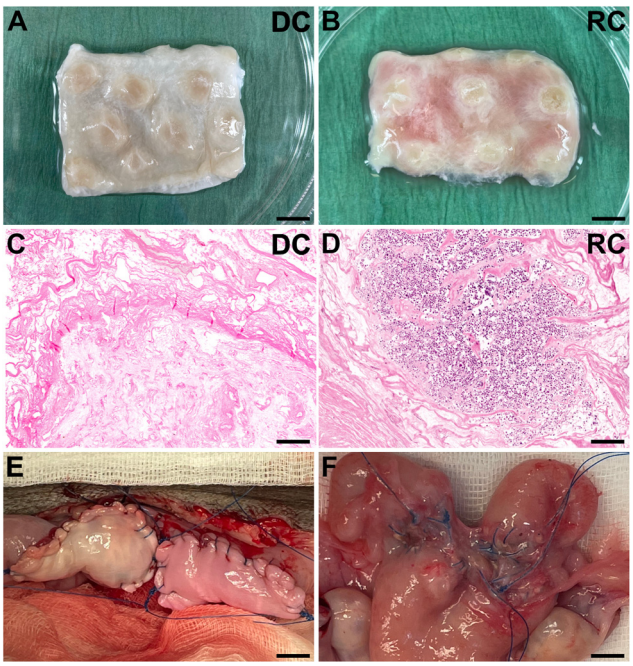

Fig. 1 After whole organ decellularization, the tissue was cut into 2 × 3 cm patches (A and B), that showed a preserved extracellular matrix, as shown after the hematoxylin and eosin staining (C). Then, half of the patches underwent a recellularization process by injecting fetal sheep bone marrow-derived stem cells (D), showing colonization of cells after 14 days of incubation. The patches were transplanted by replacement of 2 × 3 cm of the native uterine tissue (E). However, a size reduction with adhesions appeared post-transplantation (F). DC: decellularized; RC: recellularized. Scale bars in A and B = 5 mm, scale bars in C = 250 μm and D = 200 μm, scale bars in R and F = 8 mm.

media which was then transferred to the scaffold by multiple injections from all angles using a 20 G syringe (100 μl per injection; Fig. 1B). The recellularized scaffolds were then incubated for 3 h at 37 °C to allow cell attachment, and later more cell culture media was provided that completely immersed the recellularized scaffold. Each construct was then incubated at 37 °C for two weeks on a shaker, and culture media was changed every 48 h.

2.3 Bioengineered uterus patch transplantation

Recipients (n = 10) were of the same mixed sheep breed and age as the donor animals and were purchased from a local accredited supplier. All procedures related to the transplantation had been reviewed and approved by the local animal ethics committee in Gothenburg, Sweden (document 22/586). The animals were kept together in an indoor pen with free outdoor access during daytime and had free access to water and hay. The animals were also fed twice a day with concentrated pellets. The first five sheep received one graft per uterus (a decellularized tissue graft, DC, n = 2; or a recellularized tissue graft, RC, n = 3). The last five sheep received two grafts per animal, one DC and one RC on respective uterus horn (ESI Fig. 1B†). For the surgery, each animal was premedicated with analgesics and sedating medication (6–8 mg kg^{-1}, Propofol, Orion pharma animal health, Sweden, Danderyd; 0.01 mg kg^{-1} Dexidomitor, Orion Pharma Animal Health) and was continuously medicated during the surgery (0.010 mg kg^{-1} Antisedan, Orion pharma animal health, 45 minutes after Dexitdomitor; 0.03 mg mg^{-1} Vetergesic, Orion Pharma animal health; 1 mg kg^{-1} Metacam, Boehringer ingelheim animal health, Copenhagen, Denmark; 15 mg kg^{-1} Vetrimoxin, Ceva animal health, Lund, Sweden). The animals were intubated and placed in a Trendelenburg position during surgery, and to acquire necessary access to the pelvis, the rumen was emptied by the aid of a gastric tube. The abdomen was shaved and disinfected with chlorohexidine, and all the following procedures were performed under sterile conditions. A 15 cm long subumbilical, midline incision was made through the skin, muscle layer and fascia. A retractor kept the abdominal incision open, and the intestines were held back manually. The uterus was localized with a ruler and monopolar cautery outlining the incision area. A 2 × 3 cm full-thickness uterine tissue segment on the antimesenteric side of the uterus was removed. To limit tissue damage in the graft area, only major bleeding was stopped using bipolar cautery. All bioengineered uterine grafts were kept in a buffered L-15 cell culture medium, supplemented with 10% FBS and 1% Anti-Anti™ (Thermo Fisher Scientific) at 37 °C while the animal was prepared for surgery. Every graft was attached to the recipient uterus by placing a single suture in each corner of the patch (4-0 nonabsorbable suture; VP813X; Coviden, Dublin, Ireland). The sides were then attached with running sutures. The organs and bowels were then rinsed with 37 °C NaCl (0.9%) and excess blood was removed. The fascia was closed with a double Maxon™ monofilament 0-0 (Covidien) continuous suture. The subcutaneous tissue was closed with interrupted sutures (2-0, VCP317H; Ethicon, Raritan, USA) and the final skin layer was closed by continuous intracutaneous sutures using 4-0 SC644 (Covidien). Local pain relief, by sc injection of xylocaine at several sites of the incision area, was provided before the animal was allowed to wake up. Post-operative analgesics were administered intramuscularly after six hours, the following morning, and 24 hours post-surgery. Additional analgesics (1 mg kg^{-1}, Metacam, Boehringer Ingelheim, Ingelheim/Rhein, Germany) were administered every morning for four days post-surgery.

2.4 Sample collection

The experiment was terminated six weeks after the initial transplantation, and the uterus from every animal was harvested. Biopsies (0.5 cm^2) from each graft were isolated and cleaned from host tissue and preserved in RNAlater (Sigma-Aldrich) for future gene expression analysis. The remaining graft was placed in formalin and was later processed for histological and immunohistochemistry-related analysis. Blood samples were taken from the jugular vein of each experimental animal and collected in K_2EDTA gel tubes (Vacuette®, Thermo Fisher Scientific) on days 0, 3, 7, 14, and six weeks after transplantation. These blood samples were further processed for isolation of peripheral blood mononuclear cells (PBMCs) by density gradient centrifugation using Ficoll-Paque™ PLUS (Cytiva, Uppsala, Sweden). Briefly, peripheral blood was first diluted with dPBS (ThermoFisher Scientific) at a ratio of 1 : 1 and centrifuged on Ficoll-Paque™ PLUS at 400g for 35 min at room temperature. The cells from the interface (buffy coat) were collected and washed twice with washing media (RPMI 1640 supplemented with 5% FBS) at 300g for 10 min at room temperature. Finally, PBMCs were resuspended in FBS and mixed (1 : 1) with freezing media (RPMI 1640, FBS, and DMSO at a ratio 3 : 5 : 2) before freezing at −150 °C and cryopreservation until further use.

2.5 Histology and immunohistochemistry

Formalin-fixed biopsies from decellularized sheep uterus tissue, recellularized scaffolds, and grafted tissue were dehydrated in ethanol/xylene baths, paraffin-embedded, and cross-sectioned at 5μm using a microtome (HM355S; Thermo Fisher Scientific). Sections were then mounted on slides and rehydrated before further staining procedures.

Confirmation of DNA removal (after decellularization), success of *in vitro* recellularization in the patches, and the general morphology of the grafts post-transplantation were investigated by light microscopy after hematoxylin & eosin staining (H&E; Histolab, Mölndal, Sweden). In addition, standard protocols were used for Verhof-van Gieson (VVG) and Masson's trichrome (MT) staining to detect elastin and collagen, respectively, in grafts six weeks post-transplantation. Collagen was quantified using eight random fields at 400×. The area of collagen fibers was measured using Image J following a previously established method.[28] Further, we established a 4-graded scoring system using an ordinal scale for the evaluation of graft quality six weeks post-transplantation, following fundamental principles for valid scoring outlined elsewhere.[29]

Briefly, clear cut-off points were first set and defined for each grade based on tissue structure, endometrial and myometrial development, and gland formation and distribution. Based on H&E and MT histology of the uterine layers and structure, the samples were scored in order of regenerative outcomes where 0 = no or very minor regeneration (degraded and non-uniform graft structure/morphology with an indistinguishable endometrium, myometrium and glandular structure); 1 = partial regeneration (uniform graft structure/morphology with an indistinguishable endometrium, myometrium and glandular structure); 2 = substantial regeneration (uniform graft structure/morphology with a distinguishable, yet incompletely organized endometrium, myometrium and glandular structure); and 3 = major regeneration (uniform graft structure/morphology with well-defined tissue layers, including uniformly distributed glands). Each graft was scored from multiple sections by two people blinded to the study groups. For immunohistochemistry, an antigen retrieval step was performed with citrate buffer (pH = 6) in a pressure cooker. Primary antibodies (from Abcam, Cambridge, UK, unless stated otherwise) against progesterone receptor (PR, Ab101688; 1 : 500), CD31 (Ab182981; 1 : 500), CD45 (Ab10558; 1 : 800), and CD4 (Ab237722; 1 : 1000) were used together with a MACH 3™ polymer detection kit and the subsequent vulcan fast red detection kit, according to the manufacturer's instructions (Biocare Medical, Pacheco, CA, USA). Additional primary antibodies against vimentin (Ab8978; 1 : 500), smooth-muscle cell actin (αSMA, ab32575; 1 : 500), cytokeratin (Ab9377; 1 : 1000), and estrogen-alpha receptor (ERα, Ab32063; 1 : 100) were used for fluorescent immunohistochemistry. The primary antibody was incubated overnight in 4 °C and then further conjugated with a secondary fluorescent antibody (Ab150088; 1 : 300 or Ab150080; 1 : 300). The quantification of CD31+ endothelial cells in blood vessels and CD45+ and CD4+ infiltrating cells were performed manually on blinded samples where positive stained cells were counted in six random regions at 400× magnification (each region = 50 334 μm^2).

2.6 Gene expression analysis

Total RNA was extracted from biopsies preserved in RNA later (n = 37) using the RNeasy plus micro kit (Qiagen, Hilde n, Germany) and measured in a NanoDrop One (Thermo Fisher Scientific). Reverse transcription was performed using the iScript cDNA synthesis kit (BioRad, Stockholm, Sweden) and the C1000 Touch Thermal Cycler (BioRad). Digital droplet PCR mixtures were converted to droplets using QX200™ droplet generation oil for Probes (BioRad) and the QX200 droplet generator (BioRad). Finally, droplet-partitioned samples were amplified in the C1000 Touch Thermal Cycler (BioRad) and fluorescence was measured by the QX2000 droplet reader (BioRad). Data was analyzed using the QuantaSoft™ software (BioRad). Negative and positive droplets were detected, and the number of copies per µl was normalized with the reference gene before transforming data to fold change (FC). Data was presented as the ratio between study groups (DC and RC) and the paired normal uterine tissue (control group). All steps followed the manufacturer's instructions and the MIQE guidelines for ddPCR.[30]

Hydrolysis probes were designed using Beacon Designer™ software (Premier Biosoft International, San Francisco, CA, USA), synthesized by Integrated DNA technologies (specific sequences presented in ESI Table 1†) and *in vitro* validated using serial dilutions. Target genes were progesterone receptor (*PGR*), estrogen receptor 1 (*ESR1*), homeobox A10 (*HOXA10*), vascular endothelial growth factor (*VEGF*), von Willebrand factor (vWF), interferon gamma (*IFNG*), fibroblast growth factor 2 (*FGF2*), and tumor necrosis alpha (*TNFA*). Peptidyl–prolyl *cis–trans* isomerase H (*PPIH*) was used as reference gene.

2.7 FACS analysis

For cell surface staining, PBMCs were thawed and first incubated with primary antibodies for anti-sheep CD16 or CD45R (ESI Table 2†) for 20 min at 4 °C in the dark. Following two washes, a second anti-IgG1 antibody conjugated with BV421 was added and cells were incubated for 20 min in the dark at 4 °C. Finally, PBMC were washed and stained with anti-sheep monoclonal antibodies (CD14, NKp46, CD68, CD25, MHC2, CD4, and CD8; ESI Table 2†) for 20 min in the dark at 4 °C. After two washes, the cells were resuspended in FACS buffer until the analysis. For intracytoplasmic markers, surface-stained cells were fixed, permeabilized, and incubated with monoclonal antibodies (FOXP3; ESI Table 2†). The samples were analyzed on a BD FACS Melody (BD Biosciences), which includes BD FACSChorus software. Finally, all data was analyzed with FlowJO software (Tree Star, Ashland, OR). The gating strategy employed the fluorochrome minus one technique, wherein the samples were stained with all antibodies used in the assay, encompassing all fluorochromes except for one. Two animals were excluded from the FACS analysis due to having two grafts in the same recipient animal that scored different from each other, making a systemic immune response comparison between the successful and non-successful grafts difficult (animals scored as minor-partial regeneration (0–1), n = 5; animals scored as substantial-major regeneration (2–3), n = 3).

2.8 Statistics

GraphPad Prism 9 (GraphPad, CA, USA) was used for the statistical evaluation. To assess sample distribution within each group, the Shapiro–Wilk test was used. For parametric data with more than two groups, the one-way ANOVA with Tukey's corrections was applied and the results were presented as mean ± standard error of mean (SEM). For non-parametric data with more than two groups, the Kruskal–Wallis test and Dunn's *post hoc* test were used and the data reported as median ± standard deviation (SD). For parametric data with only two groups, the Welch's t-test was used, and Mann–Whitney U-test was used for non-parametric data when two groups were compared. Significance was considered when $p < 0.05$.

3. Results

3.1 General evaluation of the grafts

Histology analysis of the grafts before transplantation confirmed that the grafts were free from donor cells, had a preserved ECM architecture and were effectively recolonized with SF-SCs and cultured for 14 days of *in vitro* (Fig. 1). After transplantation, no macroscopic discrepancies were observed between the DC and the RC grafts (Fig. 1E). None of the grafted horns were affected by stenosis or fluid buildup. The extent of graft adhesions to the surrounding omentum and intestinal tissue was significant, yet, similar between the two graft types. Furthermore, grafts maintained their physical structure, displaying no intrauterine adhesions or collapse throughout the study period. However, a subset of grafts exhibited a folded structure formation due to self-adherence on the superficial layer of the graft, and a gradual degradation with a reduced graft size six weeks after transplantation (Fig. 1F).

3.2 Regenerative outcomes following an acellular or a recellularized graft

H&E staining revealed a good integration between the grafts and the surrounding native tissue six weeks post-transplantation in both study groups. Evaluation of the myometrial compartment using fluorescently stained αSMA and vimentin showed no major differences between the experimental groups (Fig. 2A–C), but there was a large intra-group variance. Cytokeratin staining indicated a successful regeneration of the luminal epithelial layer grafts from both groups (Fig. 2D–F), and most grafts exhibited a well-organized glandular structure positive for ERα and PR (Fig. 2G–L). Additional staining methods demonstrated preserved elastin and collagen structures (ESI Fig. 2A–F†). Collagen quantification revealed a significant increase in the grafts compared with native tissue (ESI Fig. 2G†).

Assessment of angiogenesis and re-vascularization using the CD31 marker indicated a significantly higher number of blood vessels in the transplants compared with native tissue, but no difference was observed between the groups (ESI Fig. 3†). Furthermore, both graft types led to an increase in both CD45+ leukocyte, and CD4+ T-cell infiltration compared with native tissue, and there were few differences in the analyzed gene expression between the groups (ESI Fig. 3†).

No clear distinction in regenerative score was evident between the two experimental groups (Fig. 3; DC = 1.57 *vs.* RC = 1.38). Nevertheless, in the DC group, three out of seven grafts were classified as "substantially regenerated" (3/7) and one graft was "comparable to normal tissue" (1/7). In contrast, five grafts (5/8) in the RC groups reached "partial regeneration", while none (0/8) were classified as "substantial regeneration", and two grafts (2/8) were "comparable to normal tissue" (Fig. 3). In order to evaluate underlying potential mechanisms that could impact the regenerative outcomes of the grafts, we decided to divide the grafts into two categories: minor regenerative outcome (scores 0 and 1; $n = 9$) and major regenerative outcome (scores 2 and 3; $n = 6$). Subsequent data analysis was conducted based on these two new study groups.

3.3 Differences between the minor and the major regenerated grafts

Analysis of the uterine layers revealed that grafts with a higher regenerative score had a more uniform, well-developed and defined muscular layer (αSMA positive staining) compared to grafts with a lower regeneration score. Vimentin was positive and well distributed in most grafts, regardless of the score (Fig. 4A–C). Cytokeratin staining showed a positive and well distributed luminal epithelial layer in all graft that was similar to native tissue, regardless of the regenerative score (Fig. 4D–F).

Elastin and collagen staining revealed that the organization of these structures appeared more structured in grafts with higher levels of regeneration (Fig. 4G–L). Further quantification of the collagen revealed higher amounts in all grafts compared with native tissue, regardless of the regeneration scores (Fig. 5A).

Evaluation of angiogenesis and re-vascularization using the CD31 marker indicated no differences based on the regenerative score (Fig. 5B). Gene expression values of *ESR1* revealed a significantly lower expression in the minor regeneration group, as compared to both native tissue and the major regeneration group and *HOXA10* also followed a similar trend (Fig. 6A–C and ESI Table 5†). For genes with pro-angiogenic functions, *vWF* showed significant upregulation in the major regeneration, while *FGF2* was significantly reduced in the minor regeneration group, in both cases compared to the native tissue, the *VEGF* levels remained unchanged (Fig. 6D–F). Expression values of the pro-inflammatory factors *TNFA* and *IFNG* also remained stable (Fig. 6G and H).

3.4 The immune response in correlation with the regenerative score

The leukocyte infiltration was significantly higher in the grafts that were classified with a minor regeneration score compared with native tissue. The major regeneration group showed a trend towards the same, but this was not significantly different compared with native tissue (Fig. 7A). The infiltration of CD4+ T-cells was significantly more in both regenerative groups.

Due to the lack of other available antibodies for immunohistochemistry on sheep immune cells for histological samples, we had to rely on the more accessible sheep antibodies used for flow cytometry analysis and the identification of circulating blood cells. Note here that two sheep presented diverging regeneration scores from their respective grafts. Hence, they were excluded from this analysis. The results showed that the total circulating CD4+ T-cell population represented a significantly higher proportion of the total PBMC population in the group that was scored with major regeneration (Fig. 7C). The total CD8+cytotoxic T-cell population showed no differences between the groups (Fig. 7D). However, when analyzing subpopulations of each subtype of T-cells (naive, activated, and effector memory re-expressing CD45RA cells; EMRA cells), the percentage of naive CD4+ and CD8+

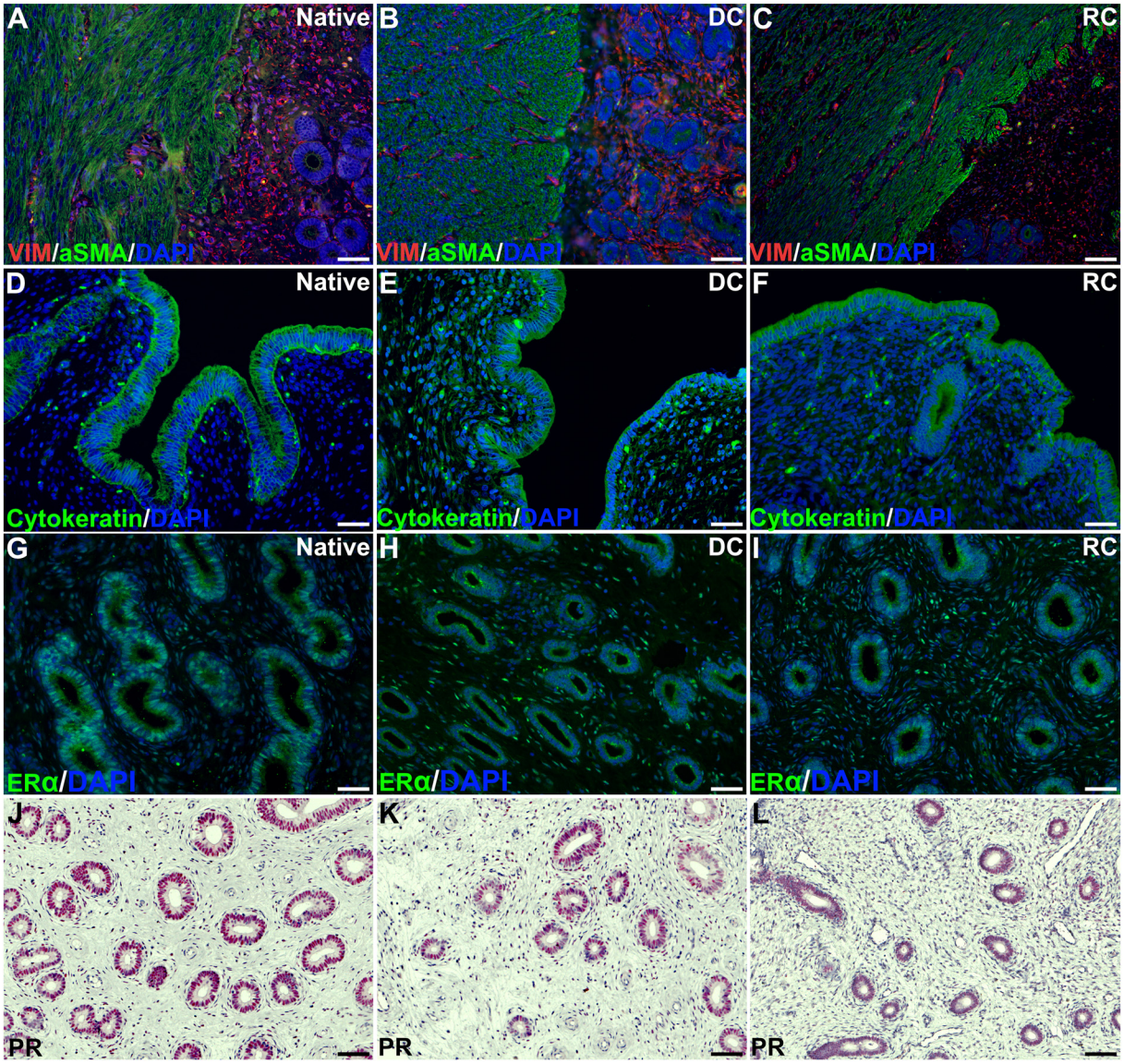

Fig. 2 Co-immunolocalization of VIM and aSMA (A–C) showed and organized endometrial stroma limiting with the myometrium, while cytokeratin (D–F) revealed a well-organized endometrial epithelium. Two hormonal receptors, ERa (G–I) and PR (J–L) were detected in the endometrial glands. DAPI: 4′,6-diamidino-2-phenylindole; ERa: estrogen receptor; PR: progesterone receptor; aSMA: alpha smooth muscle actin: VIM: vimentin. Scale bars in A–I = 45 μm, scale bars in J–L = 60 μm.

T-cells were significantly higher in the animals with successfully regenerated grafts compared with poorly regenerated grafts (Fig. 7E and F) and the opposite relation for the activated T-cells and EMRA T-cells, where grafts with poor regeneration had higher proportions than the group with better transplantation outcomes (Fig. 7G–J). The proportion of circulating CD14+ monocytes and CD14+ CD16− classical monocytes were stable between the groups during the first two weeks following transplantation, but there was a trend towards the end of the experiment that the proportion of these cell types increased in the animals with unsuccessful grafts (ESI Fig. 4A and B†). The CD14+CD16+ non-classical monocytes and Foxp3+ T_{reg} remained invariable among groups and across the experimental time (ESI Fig. 4C and D†).

4. Discussion

In this study, we extended the translational relevance of previous uterus bioengineering research that, to date, only used small animal models for *in vivo* proof-of-concept studies.[8,31] Herein, the methodology was applied to the sheep model with a uterine size similar to the human. Our primary objective was to evaluate the feasibility of a bioengineered uterus patch for a tissue replacement therapy in a large animal model, a strategy that may ultimately result in a new fertility restauration treatment for women with acquired uterine defects. Distinct from earlier studies, we herein applied relatively large grafts (6 cm^2) that, despite entailing bigger challenges regarding vascularization of the transplanted tissue,[32] are more clinically relevant

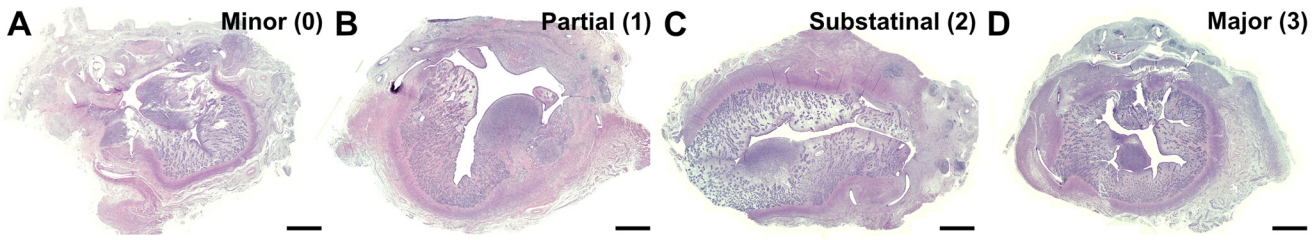

E Scoring of tissue regeneration

Group	Minor (0)	Partial (1)	Substantial (2)	Major (3)	Average score
DC	1	2	3	1	1.57
RC	1	5	0	2	1.38

(0) – Minor; Degraded and non-uniform graft structure/morphology. Tissue layers (endometrium, myometrium) not distinguishable. No uniformly distributed glands.

(1) – Partial; Uniform graft structure/morphology. Tissue layers (endometrium, myometrium) are not distinguishable. No uniformly distributed glands.

(2) – Substantial; Uniform graft structure/morphology. Tissue layers (endometrium, myometrium) are distinguishable with uniformly distributed glands. The myometrium is not completely structured.

(3) – Major; Uniform graft structure/morphology. Tissue layers are distinguishable with uniformly distributed glands. The myometrium is completely structured. Comparable to normal tissue.

Fig. 3 Representative morphology of grafts post-transplantation according to the regenerative score (A–D) and the results of scoring (E). Detailed definitions of the established scoring system to evaluate tissue regeneration. The scoring of tissue regeneration was organized into four levels (minor, partial, substantial, and major) according to the general morphology aspect. Scale bars A–D = 1500 μm.

because of their size. Therefore, we demonstrated progress towards application in the human while also highlighting current bioengineering challenges.

An earlier uterus bioengineering study in the rat showed that MSCs enhanced tissue regeneration by modulating the immune microenvironment.[18] Hence, about half the grafts in our study included SF-SCs with a confirmed MSCs cell phenotype.[26] Our recellularization methods resulted in a high cell density within the large sheep scaffolds, likely due to improved control over the cell injection methodology and cell retention as compared with our previous studies on smaller rat and sheep scaffolds.[18,25,26,33] However, the observed intragroup heterogeneity after transplantation made it challenging to directly compare study groups. Rather, other mechanisms seem to have influenced the regenerative outcomes, possibly concealing any favorable effects from the grafted SF-SCs.[34,35] Thus, the effect of the added stem cells on the scaffolds was not as noticeable as we previously observed in our rat model.[18]

Despite being a qualitative observation, the reduction of graft size after transplantation in most animals cannot be dismissed. It might indicate necrosis or scaffold degradation within the host environment, events that must be balanced with ongoing successful repair mechanisms.[34] Yet, it is important to note that several grafts in both groups (DC and RC) showed a remarkable recovery, with well-structured myometrial, endometrial, and glandular structures, including gene expression markers for tissue-specific hormone receptors. However, some grafts had less favorable regenerative outcomes. To determine what may have caused these different outcomes, we implemented a rigorous tissue scoring system by considering established histopathologic scoring guidelines[29] to evaluate uterine layer morphology and gland distribution. This scoring system allowed us to group the grafts based on the regenerative outcomes and search for possible underlying mechanisms that resulted in successful regeneration (grafts with major regeneration) or unsuccessful regeneration (grafts with minor regeneration). It is also remarkable how none of the grafts showed intrauterine adhesions since this is a common complication following uterine surgery. Still, the observed intestinal-graft adhesions to the perimetrial side of the uterus should not be dismissed. Hence, technical surgery improvements may improve outcomes, including the use of an anti-adhesive membrane[36] or developing suture-free approaches with bioadhesive hydrogels.[37,38]

Histological analysis revealed distinct graft characteristics. In the group showing good regeneration, αSMA staining and vimentin showed a better structured myometrial and endometrial layer compared with grafts with poor regeneration. The luminal epithelium closely resembled the native architecture in all grafts, suggesting that the native luminal epithelium migrates and repopulates the grafts which correlates to earlier observations in rodents.[17,39] Furthermore, endometrial glands stained positive for ERα and PR, indicating that the machinery for tissue hormone responsiveness which is critical for physiological function is present.[40] Additional histological differences between the grafts included a more normal distribution of elastin and collagen in successfully regenerated grafts, and that there was an accumulation of collagen fibers in grafts with poor regenerative outcomes, suggesting potential fibrosis and an abnormal wound-healing response.[41]

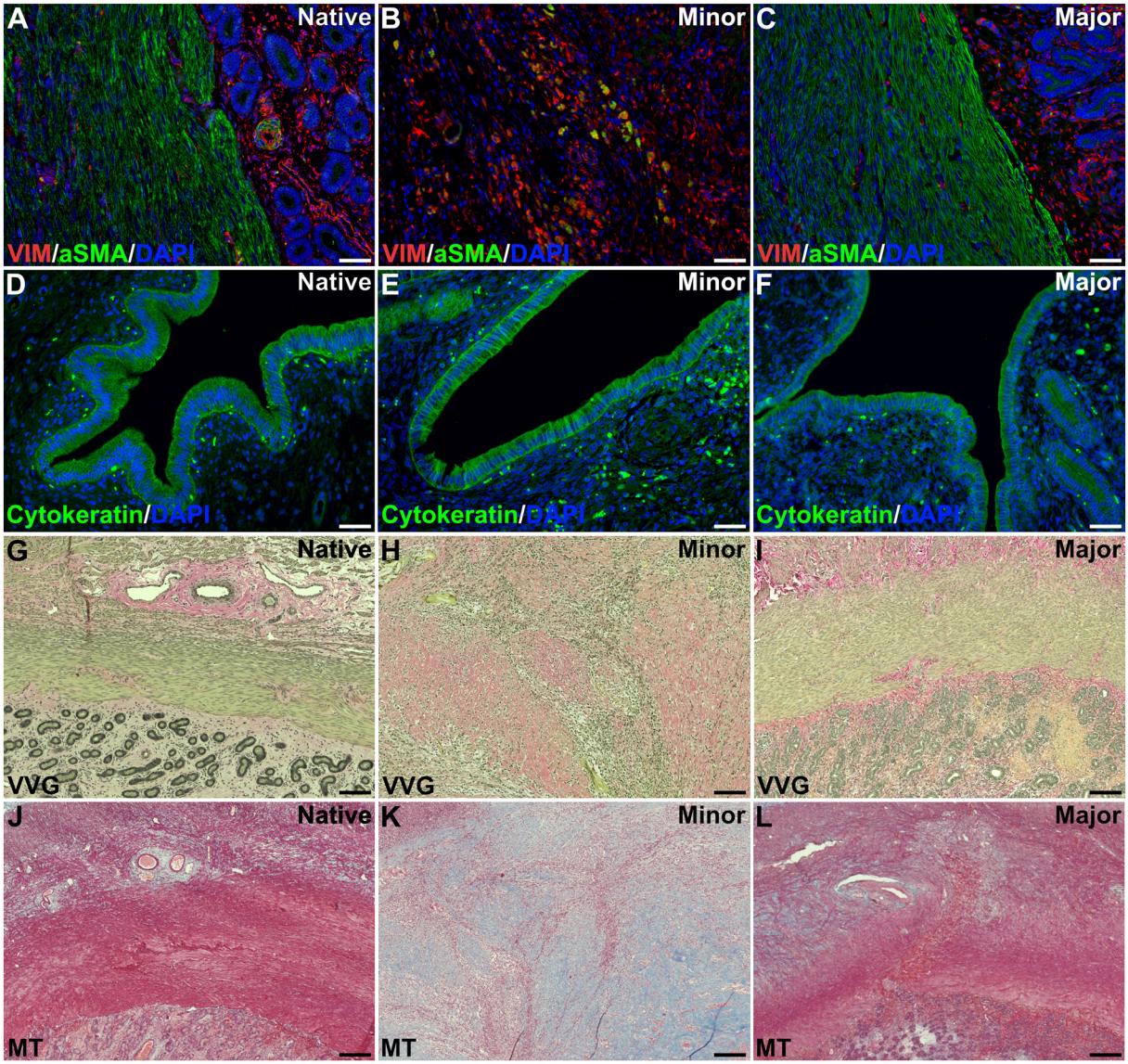

Fig. 4 Co-immunolocalization of VIM and aSMA (A–C) showed organized myometrium with the stroma in the major regeneration group (B), while cytokeratin (D–F) revealed a well-organized endometrial epithelium. The myometrial and endometrial compartments were more organized and similar to native tissue in the major regeneration group when visualized with VVG (G–I) and MT (J–L). DAPI: 4′,6-diamidino-2-phenylindole; aSMA: alpha-smooth muscle actin, VIM: vimentin, VVG: Verhoeff-Van Gieson, MT: Masson's trichrome. Scale bars in A–F = 45 μm, scale bars in G–L = 125 μm.

Furthermore, gene expression analysis revealed restored *ESR1* levels in the better regenerated grafts compared with the unsuccessfully regenerated grafts. A similar trend was also seen for the *PGR* gene. These findings suggest a gene expression pattern closer to the native tissue in the successfully regenerated grafts. Nevertheless, variations in tissue samples were noted, perhaps explained by the presence of non-glandular caruncular areas (embryo implantation sites) and glandular intercaruncular areas in the sheep uterus that were shown to have different gene expression tissue profiles.[42]

When we assessed the immune response following engraftment of bioengineered tissue, it is important to note that leukocyte infiltration is not inherently detrimental, as a higher proportion of pro-regenerative immune cells *e.g.*, M2 macrophages, is beneficial for tissue regeneration.[43] The CD45+ leukocyte infiltration and the CD4+ T-cells infiltration was similar between the successful and less successful grafts. However, our analysis provided limited insights since a comprehensive assessment, including the leukocyte subgroups, was not possible due to the limited availability of sheep antibodies for immunohistochemistry. This limitation of pre-existing analytical tools for the sheep model also challenged the design of ddPCR probes. Therefore, only *TNFA* and *IFNG* proinflammatory factors were studied. On the other hand, there was a better availability of antibodies for FACS analysis. This allowed us to conduct a detailed examination of the systemic

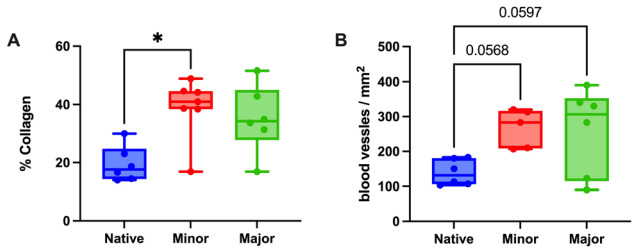

Fig. 5 The collagen fibers stained in bright blue with Masson's trichrome assay were quantified as the percentage of collagen in the total uterine area (A), entailing a significantly higher percentage in the minor regeneration group compared to the native tissue. Quantifying blood vessels (positive cells for CD31 vascular marker) revealed a trend of higher vascularization in both scored groups than in the native tissue but without differences between them (B). *$p < 0.05$.

immune cell response. Interestingly, the circulating T-cell subpopulations differed between the successful and non-successful grafts, particularly the activated CD4+ T-cells. These were of significantly higher density in animals with less successful grafts and might indicate an activated inflammatory response[44] that is associated with a higher risk of organ rejection.[45] Consistently, naïve CD4+ and CD8+ T-cells were more abundant in the successful grafts, indicating a lower T-cell activation in this group[46] and consequently a lesser graft immunogenicity.[47] Furthermore, the proportion of circulating EMRA of both CD4+ and CD8+ T-cell sub types were also higher in the animals with unsuccessful grafts, presumably relating to the higher number of activated T-cells.[48] Similar observations have previously been correlated to delayed bone

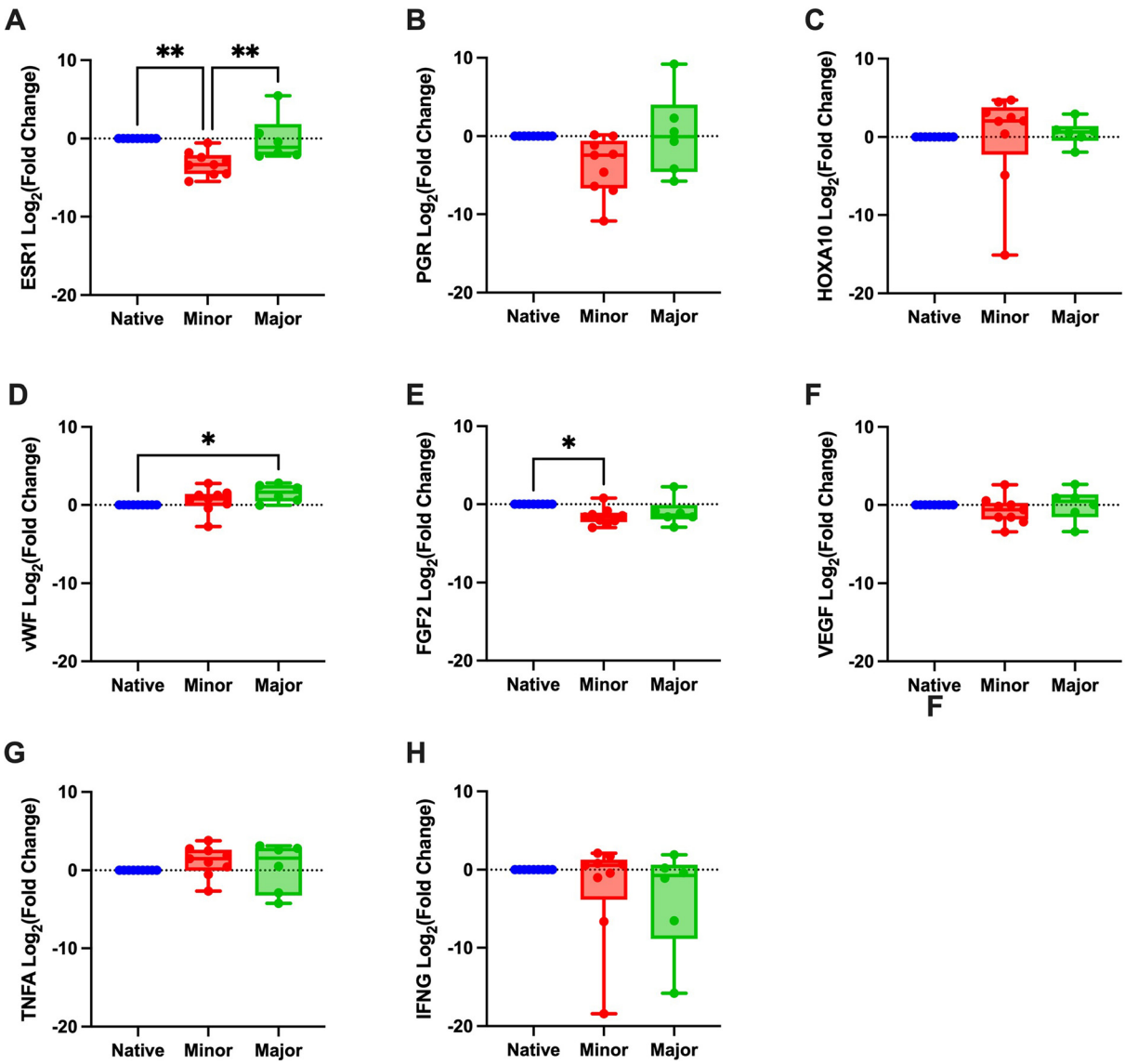

Fig. 6 Fold change, converted to $\log_2$, of both scored groups (minor and major regeneration) are calculated in relation to the native control group. Target genes were estrogen receptor 1 (ESR1; A), progesterone receptor (PGR; B), homeobox A10 (HOXA10; C), von Willebrand factor (vWF; D), fibroblast growth factor 2 (FGF2; E), vascular endothelial growth factor (VEGF; F), tumor necrosis alpha (TNFA; G), and interferon gamma (IFNG; H). *$p < 0.05$, **$p < 0.01$.

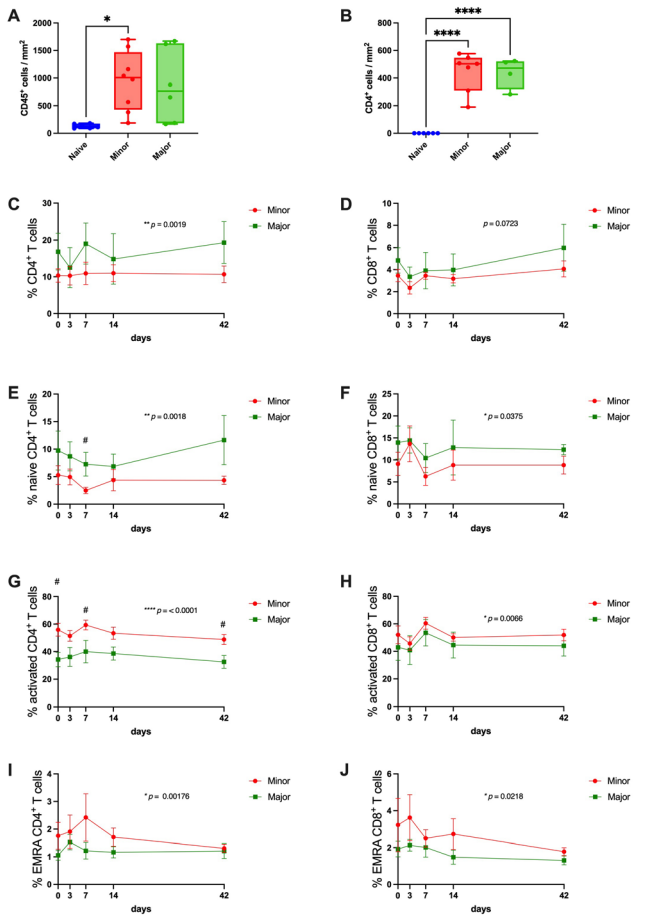

Fig. 7 Leukocyte infiltration into the tissue was confirmed by immunohistochemistry of CD45 (A) and CD4 markers (B). Local immune response evaluation was complemented with systemic immune response FACS analysis across the entire study period. The total population of CD4+ (C) and CD8+ (D) T cells were measured on days 0, 3, 7, 14, and 42 after transplantation, finding a significant difference among groups only on the CD4+ phenotype. In addition, the subpopulations of CD4+ and CD8+ T cells, referred to as naïve (E and F), activated (G and H), and EMRA (I and J), were further analyzed. Except for the activated CD8+ T cells, all T cell subpopulations showed significant differences between levels in the minor and the major regeneration groups. However, only naïve and activated CD4+ T cells showed differences across time. The *p*-values presented in C–J represents the difference between the groups during the study period, and significant differences between the groups at specific time points are indicated with "#". EMRA: effector memory RA+, FACS: fluorescence-activated cell sorting. #, significantly different at timepoint, *$p < 0.05$, ** $p < 0.01$, **** $p < 0.0001$.

healing in patients[49] and increased risk for rejection after kidney transplantation.[50] The declining levels of circulating monocytes over time in animals with unsuccessful grafts could indicate that they leave the circulation to infiltrate the grafts where they may recognize allogeneic antigens, increase the proinflammatory cytokine production and accelerate graft destruction rather than promote regeneration.[51] However, to acquire the complete overview of the immune response and the correlation between circulating and graft-infiltrating immune cells, more available antibodies would be needed for sheep tissue, which would have provided important additional information to our study. However, our results clearly show that the circulating T-cell populations significantly differed in animals with successful and non-successful grafts, and may thus, act as an indicator for the regeneration outcomes. Other factors that may have affected the study outcomes include batch variations in graft production due to the complex combination of therapies, and/or the individual animal variability, which is notably higher in the outbred sheep model compared with the specific pathogen free in-breed rat model. This variability may also extend to our cell source which was not autologous/syngeneic but was obtained from animals processed at a local abattoir for food production, typically from mixed breeds.

Still, our study provides clinically relevant data on using decellularized scaffolds for uterine repair. Previous large animal studies have shown promising transplantation results for less complex tissues such as veins[52] and arteries.[53] However, for more complex organs, results from large animal studies are sparse,[54,55] and with no focus on the regenerative or functional outcomes. Nevertheless, our study stands out by demonstrating that an implementation of an unbiased regenerative scoring system to evaluate the histological outcomes can enable important new observations. Futures studies should aim to reduce potential quality variability among the produced grafts and efforts should also be directed to validate more immune cell-specific antibodies for the sheep model so that the immune cell infiltration in the grafts can be better assessed. However, the remarkable regeneration observed in the three best-performing grafts cannot be dismissed.

5. Conclusion

This achievement, given the complexity of the uterus, provides compelling evidence that employing decellularized scaffolds for uterine bioengineering holds great promise for clinically relevant applications. Moreover, we found distinct differences in systemic T-cell subgroups between successfully regenerated grafts and those that failed. This indicates that T-cell response is crucial in determining the outcomes of uterine tissue regeneration.

Conflicts of interest

There are no conflicts to declare.

Acknowledgements

The study was financed by the Knut and Alice Wallenberg Foundation, the Swedish Research Council (VR: 116008), the ALF-agreement (between the Swedish Government and the county council), the Adlerbertska, Wilhelm & Martina Lundgrens research foundations.

We thank CCI at University of Gothenburg and the NMI (VR-RFI 2019-00217) for assistance in electron microscopy.

References

1 M. N. Mascarenhas, S. R. Flaxman, T. Boerma, S. Vanderpoel and G. A. Stevens, National, regional, and global trends in infertility prevalence since 1990: a systematic analysis of 277 health surveys, *PLoS Med.*, 2012, **9**(12), e1001356.

2 M. M. Dolmans, M. von Wolff, C. Poirot, C. Diaz-Garcia, L. Cacciottola, N. Boissel, J. Liebenthron, A. Pellicer, J. Donnez and C. Y. Andersen, Transplantation of cryopreserved ovarian tissue in a series of 285 women: a review of five leading European centers, *Fertil. Steril.*, 2021, **115**(5), 1102–1115.

3 M. Brännström, L. Johannesson, H. Bokström, N. Kvarnström, J. Mölne, P. Dahm-Kähler, A. Enskog, M. Milenkovic, J. Ekberg, C. Diaz-Garcia, M. Gäbel, A. Hanafy, H. Hagberg, M. Olausson and L. Nilsson, Livebirth after uterus transplantation, *Lancet*, 2015, **385**(9968), 607–616.

4 M. M. Laronda, Engineering a bioprosthetic ovary for fertility and hormone restoration, *Theriogenology*, 2020, **150**, 8–14.

5 M. C. Chiti, J. Vanacker, E. Ouni, N. Tatic, A. Viswanath, A. des Rieux, M. M. Dolmans, L. J. White and C. A. Amorim, Ovarian extracellular matrix-based hydrogel for human ovarian follicle survival in vivo: A pilot work, *J. Biomed. Mater. Res., Part B*, 2022, **110**(5), 1012–1022.

6 E. Francés-Herrero, R. Lopez, M. Hellström, L. de Miguel-Gómez, S. Herraiz, M. Brännström, A. Pellicer and I. Cervelló, Bioengineering trends in female reproduction: a systematic review, *Hum. Reprod. Update*, 2022, **28**(6), 798–837.

7 S. E. Pors, M. Ramløse, D. Nikiforov, K. Lundsgaard, J. Cheng, C. Y. Andersen and S. G. Kristensen, Initial steps in reconstruction of the human ovary: survival of pre-antral stage follicles in a decellularized human ovarian scaffold, *Hum. Reprod.*, 2019, **34**(8), 1523–1535.

8 E. Sehic, M. Brännström and M. Hellström, Progress in Preclinical Research on Uterus Bioengineering That Utilizes Scaffolds Derived from Decellularized Uterine Tissue, *Biomed. Mater. Devices*, 2023, **1**, 66–73.

9 K. Miyazaki and T. Maruyama, Partial regeneration and reconstruction of the rat uterus through recellularization of a decellularized uterine matrix, *Biomaterials*, 2014, **35**(31), 8791–8800.

10 M. Hellstrom, R. R. El-Akouri, C. Sihlbom, B. M. Olsson, J. Lengqvist, H. Backdahl, B. R. Johansson, M. Olausson, S. Sumitran-Holgersson and M. Brannstrom, Towards the development of a bioengineered uterus: comparison of different protocols for rat uterus decellularization, *Acta Biomater.*, 2014, **10**(12), 5034–5042.

11 E. G. Santoso, K. Yoshida, Y. Hirota, M. Aizawa, O. Yoshino, A. Kishida, Y. Osuga, S. Saito, T. Ushida and K. S. Furukawa, Application of detergents or high hydrostatic pressure as decellularization processes in uterine tissues and their subsequent effects on in vivo uterine regeneration in murine models, *PLoS One*, 2014, **9**(7), e103201.

12 G. Agmon and K. L. Christman, Controlling stem cell behavior with decellularized extracellular matrix scaffolds, *Curr. Opin. Solid State Mater. Sci.*, 2016, **20**(4), 193–201.

13 A. M. Padma, A. B. Alshaikh, M. J. Song, R. Akouri, M. Oltean, M. Brännström and M. Hellström, Decellularization protocol-dependent damage-associated molecular patterns in rat uterus scaffolds differentially affect the immune response after transplantation, *J. Tissue Eng. Regener. Med.*, 2021, **15**(7), 674–685.

14 A. M. Padma, A. B. Alsheikh, M. J. Song, R. Akouri, L. M. Akyürek, M. Oltean, M. Brännström and M. Hellström, Immune response after allogeneic transplantation of decellularized uterine scaffolds in the rat, *Biomed. Mater.*, 2021, **16**(4), DOI: **10.1088/1748-605X/abfdfe**.

15 A. M. Padma, M. Brännström and M. Hellström, Uterus bioengineering as a future alternative to uterus transplantation, *Clin. Exp. Obstet. Gynecol.*, 2022, **49**(3), 72.

16 Y. Zhang, Y. He, S. Bharadwaj, N. Hammam, K. Carnagey, R. Myers, A. Atala and M. Van Dyke, Tissue-specific extracellular matrix coatings for the promotion of cell proliferation and maintenance of cell phenotype, *Biomaterials*, 2009, **30**(23–24), 4021–4028.

17 T. Hiraoka, Y. Hirota, T. Saito-Fujita, M. Matsuo, M. Egashira, L. Matsumoto, H. Haraguchi, S. K. Dey, K. S. Furukawa, T. Fujii and Y. Osuga, STAT3 accelerates uterine epithelial regeneration in a mouse model of decellularized uterine matrix transplantation, *JCI Insight*, 2016, **1**(8), e87591.

18 E. Sehic, E. Thorén, I. Gudmundsdottir, M. Oltean, M. Brännström and M. Hellström, Mesenchymal stem cells establish a pro-regenerative immune milieu after decellularized rat uterus tissue transplantation, *J. Tissue Eng.*, 2022, **13**, DOI: **10.1177/20417314221118858**.

19 N. Charoensombut, K. Kawabata, J. Kim, M. Chang, T. Kimura, A. Kishida, T. Ushida and K. S. Furukawa, Internal radial perfusion bioreactor promotes decellularization and recellularization of rat uterine tissue, *J. Biosci. Bioeng.*, 2022, **133**(1), 83–88.

20 F. Miki, T. Maruyama, K. Miyazaki, T. Takao, Y. Yoshimasa, S. Katakura, H. Hihara, S. Uchida, H. Masuda, H. Uchida, T. Nagai, S. Shibata and M. Tanaka, The orientation of a decellularized uterine scaffold determines the tissue topology and architecture of the regenerated uterus in rats†, *Biol. Reprod.*, 2019, **100**(5), 1215–1227.

21 X. Li, Y. Wang, R. Ma, X. Liu, B. Song, Y. Duan, J. Guo, G. Feng, T. Cui, L. Wang, J. Hao, H. Wang and Q. Gu, Reconstruction of functional uterine tissues through recellularizing the decellularized rat uterine scaffolds by MSCs in vivo and in vitro, *Biomed. Mater.*, 2021, **16**(3), 035023.

22 Q. Yao, Y. W. Zheng, H. L. Lin, Q. H. Lan, Z. W. Huang, L. F. Wang, R. Chen, J. Xiao, L. Kou, H. L. Xu and Y. Z. Zhao, Exploiting crosslinked decellularized matrix to achieve uterus regeneration and construction, *Artif. Cells, Nanomed., Biotechnol.*, 2020, **48**(1), 218–229.

23 H. Campo, P. M. Baptista, N. López-Pérez, A. Faus, I. Cervelló and C. Simón, De- and recellularization of the pig uterus: a bioengineering pilot study, *Biol. Reprod.*, 2017, **96**(1), 34–45.

24 S. S. Daryabari, A. M. Kajbafzadeh, K. Fendereski, F. Ghorbani, M. Dehnavi, M. Rostami, B. A. Garajegayeh and S. M. Tavangar, Development of an efficient perfusion-based protocol for whole-organ decellularization of the ovine uterus as a human-sized model and in vivo application of the bioscaffolds, *J. Assist. Reprod. Genet.*, 2019, **36**(6), 1211–1223.

25 T. T. Tiemann, A. M. Padma, E. Sehic, H. Bäckdahl, M. Oltean, M. J. Song, M. Brännström and M. Hellström, Towards uterus tissue engineering: a comparative study of sheep uterus decellularisation, *Mol. Hum. Reprod.*, 2020, **26**(3), 167–178.

26 A. M. Padma, L. Carrière, F. Krokström Karlsson, E. Sehic, S. Bandstein, T. T. Tiemann, M. Oltean, M. J. Song, M. Brännström and M. Hellström, Towards a bioengineered uterus: bioactive sheep uterus scaffolds are effectively recellularized by enzymatic preconditioning, *npj Regener. Med.*, 2021, **6**(1), 26.

27 S. S. Daryabari, K. Fendereski, F. Ghorbani, M. Dehnavi, Y. Shafikhani, A. Omranipour, S. Zeraatian-Nejad Davani, M. Majidi Zolbin, S. M. Tavangar and A. M. Kajbafzadeh, Whole-organ decellularization of the human uterus and in vivo application of the bio-scaffolds in animal models, *J. Assist. Reprod. Genet.*, 2022, **39**(6), 1237–1247.

28 Y. Chen, Q. Yu and C.-B. Xu, A convenient method for quantifying collagen fibers in atherosclerotic lesions by ImageJ software, *Int. J. Clin. Exp. Med.*, 2017, **10**(10), 14904–14910.

29 K. N. Gibson-Corley, A. K. Olivier and D. K. Meyerholz, Principles for valid histopathologic scoring in research, *Vet. Pathol.*, 2013, **50**(6), 1007–1015.

30 J. F. Huggett, C. A. Foy, V. Benes, K. Emslie, J. A. Garson, R. Haynes, J. Hellemans, M. Kubista, R. D. Mueller, T. Nolan, M. W. Pfaffl, G. L. Shipley, J. Vandesompele, C. T. Wittwer and S. A. Bustin, The digital MIQE guidelines: Minimum Information for Publication of Quantitative Digital PCR Experiments, *Clin. Chem.*, 2013, **59**(6), 892–902.

31 R. S. Magalhaes, J. K. Williams, K. W. Yoo, J. J. Yoo and A. Atala, A tissue-engineered uterus supports live births in rabbits, *Nat. Biotechnol.*, 2020, **38**(11), 1280–1287.

32 G. Li, Q. Han, P. Lu, L. Zhang, Y. Zhang, S. Chen, P. Zhang, L. Zhang, W. Cui, H. Wang and H. Zhang, Construction of Dual-Biofunctionalized Chitosan/Collagen Scaffolds for Simultaneous Neovascularization and Nerve Regeneration, *Research*, 2020, **2020**, 2603048.

33 M. Hellström, J. M. Moreno-Moya, S. Bandstein, E. Bom, R. R. Akouri, K. Miyazaki, T. Maruyama and M. Brännström, Bioengineered uterine tissue supports pregnancy in a rat model, *Fertil. Steril.*, 2016, **106**(2), 487–496.e1.

34 P. Lu, K. Takai, V. M. Weaver and Z. Werb, Extracellular matrix degradation and remodeling in development and disease, *Cold Spring Harbor Perspect. Biol.*, 2011, **3**(12), a005058.

35 Z. Julier, A. J. Park, P. S. Briquez and M. M. Martino, Promoting tissue regeneration by modulating the immune system, *Acta Biomater.*, 2017, **53**, 13–28.

36 M. Rottenstreich, R. Rotem, A. Hirsch, R. Farkash, A. Rottenstreich, H. Y. Sela, A. Samueloff and S. Grisaru-Granovsky, The use of absorbable adhesion barriers to reduce the incidence of intraperitoneal adhesions at repeat cesarean delivery, *Arch. Gynecol. Obstet.*, 2020, **302**(1), 101–108.

37 X. Wu, W. Guo, L. Wang, Y. Xu, Z. Wang, Y. Yang, L. Yu, J. Huang, Y. Li, H. Zhang, Y. Wu, G. Li and W. Huang, An Injectable Asymmetric-Adhesive Hydrogel as a GATA6+ Cavity Macrophage Trap to Prevent the Formation of Postoperative Adhesions after Minimally Invasive Surgery, *Adv. Funct. Mater.*, 2022, **32**(9), 2110066.

38 X. Wu, Z. Wang, J. Xu, L. Yu, M. Qin, J. Li, S. Liu, W. Zheng, Z. Li, J. Ouyang, Y. Li, G. Li, L. Wang, W. Huang and Y. Wu, Photocurable injectable Janus hydrogel with minimally invasive delivery for all-in-one treatment of gastric perforations and postoperative adhesions, *Theranostics*, 2023, **13**(15), 5365–5385.

39 J. Liu, L. E. Pascal, S. Isharwal, D. Metzger, R. Ramos Garcia, J. Pilch, S. Kasper, K. Williams, P. H. Basse, J. B. Nelson, P. Chambon and Z. Wang, Regenerated luminal epithelial cells are derived from preexisting luminal epithelial cells in adult mouse prostate, *Mol. Endocrinol.*, 2011, **25**(11), 1849–1857.

40 R. M. Marquardt, T. H. Kim, J. H. Shin and J. W. Jeong, Progesterone and Estrogen Signaling in the Endometrium: What Goes Wrong in Endometriosis?, *Int. J. Mol. Sci.*, 2019, **20**(15), 3822.

41 T. A. Wynn, Cellular and molecular mechanisms of fibrosis, *J. Pathol.*, 2008, **214**(2), 199–210.

42 Y. Wang, C. Wang, Z. Hou, K. Miao, H. Zhao, R. Wang, M. Guo, Z. Wu, J. Tian and L. An, Comparative analysis of proteomic profiles between endometrial caruncular and intercaruncular areas in ewes during the peri-implantation period, *J. Anim. Sci. Biotechnol.*, 2013, **4**(1), 39.

43 K. E. Martin and A. J. García, Macrophage phenotypes in tissue repair and the foreign body response: Implications for biomaterial-based regenerative medicine strategies, *Acta Biomater.*, 2021, **133**, 4–16.

44 N. T. Funderburg, S. R. Stubblefield Park, H. C. Sung, G. Hardy, B. Clagett, J. Ignatz-Hoover, C. V. Harding, P. Fu, J. A. Katz, M. M. Lederman and A. D. Levine, Circulating CD4(+) and CD8(+) T cells are activated in inflammatory bowel disease and are associated with plasma markers of inflammation, *Immunology*, 2013, **140**(1), 87–97.

45 A. A. Duizendstra, R. J. de Knegt, S. Mancham, M. Klepper, D. L. Roelen, S. H. Brand-Schaaf, P. P. Boor, M. Doukas,

R. A. de Man, D. Sprengers, M. P. Peppelenbosch, M. G. H. Betjes, J. Kwekkeboom and N. H. R. Litjens, Activated CD4(+) T Cells and Highly Differentiated Alloreactive CD4(+) T Cells Distinguish Operationally Tolerant Liver Transplantation Recipients, *Liver Transplant.*, 2022, **28**(1), 98–112.

46 M. Künzli and D. Masopust, CD4+ T cell memory, *Nat. Immunol.*, 2023, **24**(6), 903–914.

47 H. Waldmann, T.-C. Chen, L. Graca, E. Adams, S. Daley, S. Cobbold and P. J. Fairchild, Regulatory T cells in transplantation, *Semin. Immunol.*, 2006, **18**(2), 111–119.

48 I. Raphael, R. R. Joern and T. G. Forsthuber, Memory CD4 (+) T Cells in Immunity and Autoimmune Diseases, *Cells*, 2020, **9**(3), 531.

49 S. Reinke, S. Geissler, W. R. Taylor, K. Schmidt-Bleek, K. Juelke, V. Schwachmeyer, M. Dahne, T. Hartwig, L. Akyüz, C. Meisel, N. Unterwalder, N. B. Singh, P. Reinke, N. P. Haas, H.-D. Volk and G. N. Duda, Terminally Differentiated $CD8^+$ T Cells Negatively Affect Bone Regeneration in Humans, *Sci. Transl. Med.*, 2013, **5**(177), 177ra36–177ra36.

50 L. Jacquemont, G. Tilly, M. Yap, T. M. Doan-Ngoc, R. Danger, P. Guérif, F. Delbos, B. Martinet, M. Giral, Y. Foucher, S. Brouard and N. Degauque, Terminally Differentiated Effector Memory CD8(+) T Cells Identify Kidney Transplant Recipients at High Risk of Graft Failure, *J. Am. Soc. Nephrol.*, 2020, **31**(4), 876–891.

51 M. H. Oberbarnscheidt, Q. Zeng, Q. Li, H. Dai, A. L. Williams, W. D. Shlomchik, D. M. Rothstein and F. G. Lakkis, Non-self recognition by monocytes initiates allograft rejection, *J. Clin. Invest.*, 2014, **124**(8), 3579–3589.

52 J. Håkansson, R. Simsa, Y. Bogestål, L. Jenndahl, T. Gustafsson-Hedberg, S. Petronis, R. Strehl and K. Österberg, Individualized tissue-engineered veins as vascular grafts: A proof of concept study in pig, *J. Tissue Eng. Regener. Med.*, 2021, **15**(10), 818–830.

53 L. Jenndahl, K. Österberg, Y. Bogestål, R. Simsa, T. Gustafsson-Hedberg, P. Stenlund, S. Petronis, A. Krona, P. Fogelstrand, R. Strehl and J. Håkansson, Personalized tissue-engineered arteries as vascular graft transplants: A safety study in sheep, *Regener. Ther.*, 2022, **21**, 331–341.

54 E. C. Stahl, R. W. Bonvillain, C. D. Skillen, B. L. Burger, H. Hara, W. Lee, C. B. Trygg, P. J. Didier, B. F. Grasperge, N. C. Pashos, B. A. Bunnell, J. Bianchi, D. L. Ayares, K. I. Guthrie, B. N. Brown and T. H. Petersen, Evaluation of the host immune response to decellularized lung scaffolds derived from α-Gal knockout pigs in a non-human primate model, *Biomaterials*, 2018, **187**, 93–104.

55 A. M. Kajbafzadeh, R. Khorramirouz, B. Nabavizadeh, S. S. Ladi Seyedian, A. Akbarzadeh, R. Heidari, A. Masoumi, B. Azizi and R. Seyed Hossein Beigi, Whole organ sheep kidney tissue engineering and in vivo transplantation: Effects of perfusion-based decellularization on vascular integrity, *Mater. Sci. Eng., C*, 2019, **98**, 392–400.

